

PAPER • OPEN ACCESS

A 3D kinetic Monte Carlo study of streamer discharges in CO_2

To cite this article: R Marskar 2024 *Plasma Sources Sci. Technol.* **33** 025023

View the [article online](#) for updates and enhancements.

You may also like

- [Properties and characteristics of the nanosecond discharge developing at the water–air interface: tracking evolution from a diffused streamer to a spark filament](#)
Garima Arora, Petr Hoffer, Václav Prukner et al.
- [Fine structure resolved excitation cross sections of singly ionized Ga for the modeling and diagnostics of Ga plasmas](#)
Indhu Suresh, Priti, R Srivastava et al.
- [Absolute calibration of the ratio of Xe/O two-photon absorption cross-sections for O-TALIF applications](#)
Z Shu, N A Popov and S M Starikovskaia



Analysis Solutions for your Plasma Research

- Knowledge
- Experience ■ Expertise

[Click to view our product catalogue](#)

Contact Hiden Analytical for further details:
W www.HidenAnalytical.com
E info@hiden.co.uk



Surface Science

- ▶ Surface Analysis
- ▶ SIMS



Surface Science

- ▶ 3D depth Profiling
- ▶ Nanometre depth resolution



Plasma Diagnostics

- ▶ Plasma characterisation
- ▶ Customised systems to suit plasma Configuration



Plasma Diagnostics

- ▶ Mass and energy analysis of plasma ions
- ▶ Characterisation of neutrals and radicals

A 3D kinetic Monte Carlo study of streamer discharges in CO₂

R Marskar 

SINTEF Energy Research, Sem Sælands vei 11, Trondheim 7034, Norway

E-mail: robert.marskar@sintef.no

Received 6 December 2023, revised 19 January 2024

Accepted for publication 13 February 2024

Published 23 February 2024



Abstract

We theoretically study the inception and propagation of positive and negative streamers in CO₂. Our study is done in 3D, using a newly formulated kinetic Monte Carlo discharge model where the electrons are described as drifting and diffusing particles that adhere to the local field approximation. Our emphasis lies on electron attachment and photoionization. For negative streamers we find that dissociative attachment in the streamer channels leads to appearance of localized segments of increased electric fields, while an analogous feature is not observed for positive-polarity discharges. Positive streamers, unlike negative streamers, require free electrons ahead of them in order to propagate. In CO₂, just as in air, these electrons are supplied through photoionization. However, ionizing radiation in CO₂ is absorbed quite rapidly and is also weaker than in air, which has important ramifications for the emerging positive streamer morphology (radius, velocity, and fields). We perform a computational analysis which shows that positive streamers can propagate due to photoionization in CO₂. Conversely, photoionization has no effect on negative streamer fronts, but plays a major role in the coupling between negative streamers and the cathode. Photoionization in CO₂ is therefore important for the propagation of both positive and negative streamers. Our results are relevant in several applications, e.g. CO₂ conversion and high-voltage technology (where CO₂ is used in pure form or admixed with other gases).

Keywords: 3D, streamer, CO₂

1. Introduction

As with other gases, electric discharges in CO₂ begin with one or more initial electrons that accelerate in an electric field. If the electron velocity becomes sufficiently high, collisions with CO₂ molecules lead to net ionization when the ionization probability exceeds the attachment probability. As the process cascades through further ionization by acceleration of secondary electrons, build-up of space charge from the electrons and residual ions modifies the electric field in which the

electrons originally accelerated. This modification marks the onset of a streamer discharge [1], which is a filamentary type of low-temperature plasma. Streamers have the peculiar property that they continuously modify the electric field in which they propagate, and thus exhibit a substantial degree of self-propagation.

Streamer discharges are categorized as positive or negative, depending on their direction of propagation relative to the electric field. Negative streamers propagate in the direction of the electrons (hence opposite to the electric field), and are characterized by a negative space charge layer surrounding their channels. Streamers that propagate opposite to the electron drift direction are called positive streamers, and unlike negative streamers they require a source of free electrons ahead of them. In air and other N₂–O₂ mixtures, this source is photoionization. CO₂ is another molecule that is relevant in



Original Content from this work may be used under the terms of the [Creative Commons Attribution 4.0 licence](https://creativecommons.org/licenses/by/4.0/). Any further distribution of this work must maintain attribution to the author(s) and the title of the work, journal citation and DOI.

multiple fields of research involving electrical discharges. In high-voltage (HV) technology, for example, manufacturers of HV equipment are currently transitioning from the usage of SF₆ to environmentally friendlier alternatives, such as pure CO₂ or mixtures of CO₂ and C₄F₇N (also relevant are mixtures of air and C₅F₁₀O). However, photoionization in CO₂ is known to be much weaker than in air (for an overview, see Pancheshnyi [2]). It is now also accepted that photoionization sensitively affects the morphology of positive streamers in air [3–5] since it produces electron–ion pairs in regions where the plasma density is low, which exacerbates noise at the streamer front. Positive streamer branching thus occurs much more frequently in gases with lower amounts of photoionization [6]. Since photoionization in CO₂ is lower than in air, one may expect that positive streamer discharges propagate quite irregularly.

Few experimental studies have addressed streamer propagation in CO₂. Experiments by Seeger *et al* [7] showed that the DC breakdown voltage of CO₂ is different for positive and negative polarities. The authors investigated DC discharges in non-uniform fields for both polarities, and showed that the breakdown voltage for positive polarity is lower than for negative polarity at pressures $p \leq 1$ bar. At higher pressures $p > 1$ bar this trend was reversed, and breakdown at negative polarity consistently occurred at a lower applied voltage than breakdowns at positive polarity. This behavior is quite unlike that of air, where positive streamers propagate more easily than negative streamers over a wide range of pressures. Large statistical time lags were also observed for positive streamers, but not for negative streamers. Inception did not always occur for positive streamers, despite waiting times up to several minutes, indicating that initiatory electrons are quite rare in CO₂. No similar effect was reported for negative streamers, which suggests that the source of the initiatory electron could be different for the two polarities. A more thorough investigation of inception times in CO₂ was recently presented by Mirpour and Nijdam [8], who investigated pulsed discharges with 10 Hz repetition rates.

Theoretically, Levko *et al* [9] studied streamer propagation in CO₂ gas using a particle-in-cell (PIC) model with Monte Carlo collisions (MCC), ignoring photoionization and elucidating the intricate details of the electron velocity distribution. Bagheri *et al* [10] studied positive streamers in CO₂ and air using a fluid model. For CO₂, the authors claim that photoionization is an irrelevant mechanism, and in the computer simulations they replace it by a uniform background ionization. The above theoretical studies were done in Cartesian 2D [9] and axisymmetric 2D [10], and 3D simulations have not yet been reported.

In this paper we study the formation of positive and negative streamer discharges in pure CO₂, in full 3D. Our focus lies on the emerging morphology of the streamers, and in particular on the roles of electron attachment and photoionization. We show that currently reported photoionization levels for CO₂ [2] can facilitate positive streamer propagation. As we artificially decrease the level of photoionization, we find that higher voltages are required in order to initiate positive streamer discharges. Negative streamers are also examined, and we show

that the comparatively low levels of photoionization in CO₂ has virtually no effect on the dynamics of negative streamer heads. However, photoionization is shown to play a role in the coupling of the negative streamer to the cathode.

This paper is organized as follows: our computational model is presented in section 2, where we include the physical model and a brief overview of the numerical discretization that we use. Results are presented in section 3.1 and section 3.2 for negative streamers, and in sections 3.3 and 3.4 for positive streamers. The paper is then concluded in section 4.

2. Theoretical model

2.1. Physical model

We use a physical model where the electrons are described as microscopic particles that drift and diffuse according to the local field approximation (LFA), i.e. we use a microscopic drift-diffusion model rather than a fluid drift-diffusion model [11]. The transport equation for the electrons occurs in the form of Itô diffusion:

$$d\mathbf{X} = \mathbf{V}dt + \sqrt{2D}d\mathbf{N}, \quad (1)$$

where $\mathbf{X}(t)$ is the electron position, and \mathbf{V} and D are the electron drift velocity and diffusion coefficient. \mathbf{N} indicates a normal distribution with a mean value of zero and a standard deviation of one, and we close the velocity relation in the LFA as

$$\mathbf{V} = \mathbf{v}_e(\mathbf{X}), \quad (2)$$

$$D = D_e(\mathbf{X}), \quad (3)$$

where $\mathbf{v}_e = -\mu_e \mathbf{E}$ is the fluid drift velocity where μ_e is the electron mobility and \mathbf{E} is the electric field, and D_e is the fluid diffusion coefficient. Our model is quite similar to a conventional macroscopic drift-diffusion model, except that we replace the electron transport kernel by a microscopic drift-diffusion process (i.e. an Itô process) and the reactions by a kinetic Monte Carlo (KMC) algorithm. Thus, the electrons in our model adhere to the same transport process as in conventional LFA-based fluid methods, with the important distinction that they move and react stochastically. Further details regarding the Itô-KMC algorithm and its association with fluid drift-diffusion models is given in [11].

We use a fluid drift-diffusion model for ions, whose densities are indicated by n_i where i is some species index. The equation of motion for the ions is

$$\frac{\partial n_i}{\partial t} = -\nabla \cdot (\mathbf{v}_i n_i - D_i \nabla n_i) + S_i. \quad (4)$$

where \mathbf{v}_i , D_i , and S_i are the drift velocities, diffusion coefficients, and source terms for ions of type of i . The electric field $\mathbf{E} = -\nabla \Phi$ is obtained by solving the Poisson equation for the potential Φ :

$$\nabla^2 \Phi = -\frac{\rho}{\epsilon_0}, \quad (5)$$

Table 1. CO₂ plasma chemistry used in this paper.

Reaction	Rate	reference
$e + \text{CO}_2 \rightarrow e + e + \text{CO}_2^+$	$k_\alpha(E/N)$	[14]
$e + \text{CO}_2 \rightarrow \text{CO} + \text{O}^-$	$k_\eta(E/N)$	[14]
$e + \text{CO}_2 \rightarrow e + \text{CO}_2 + \gamma$	$k_\gamma(E/N)$	[14]

where ρ is the space charge density and ϵ_0 is the vacuum permittivity.

2.2. Chemistry

We consider a comparatively simple kinetic scheme for CO₂ consisting only of ionizing, attaching, and photon-producing reactions, see table 1. Excited states of CO₂ are not tracked in our model as we are presently only interested in the main ion products. We also remark that while the KMC algorithm uses chemical propensities rather than the more conventional reaction rate coefficient, all reactions in this paper are first-order reactions and in this case the reaction rates in the KMC and fluid formulations are numerically equivalent. The connection between the rates that occur in the chemical propensities and conventional reaction rates can otherwise be quite subtle for higher-order reactions, see e.g. [11–13] for further details.

Transport coefficients and reaction rates for the electrons are computed using BOLSIG+ [14] and the Phelps database (retrieved 16 October 2023) [15]. The ion mobility is set to $2 \times 10^{-4} \text{ m}^2 (\text{Vs})^{-1}$. All rates are calculated at standard atmosphere, i.e. $N \approx 2.446 \times 10^{25} \text{ m}^{-3}$.

2.3. Electron attachment in CO₂

In the transport data we notice a peculiar feature that is relevant on longer timescales (tens of nanoseconds). Figure 1 shows the ionization and attachment coefficients (k_α and k_η), and the effective ionization rate ($k_\alpha - k_\eta$) for the attachment region $E/N \leq 90 \text{ Td}$. For fields $E/N \approx 70 \text{ Td}$ there is a global minimum in the effective ionization coefficient where dissociative attachment is particularly effective. At atmospheric pressure, which is what we study, the attachment lifetime at $E/N \approx 70 \text{ Td}$ is $1/|k_\alpha - k_\eta| \approx 20 \text{ ns}$. If such fields appear in the streamer channel, dissociative attachment can potentially reduce the electron density by a factor of $1/e$ every 20 ns. We mention this feature because an analogous phenomenon exists for streamer discharges in air, where it is known as the attachment instability [16].

The physical explanation of the attachment instability is based on the tendency of streamer channels to become quasi-stationary due to the short relaxation time of the channel, in which case the current through the channel is constant [17]. We then obtain $\nabla \cdot (\sigma \mathbf{E}) = 0$ for the current density $\mathbf{J} = \sigma \mathbf{E}$, where σ is the electric conductivity. When electron attachment reduces the conductivity the channel responds by increasing the electric field such that the current through the channel remains constant. Because the effective attachment rate is field dependent with a local maximum around $E/N \approx 70 \text{ Td}$, this

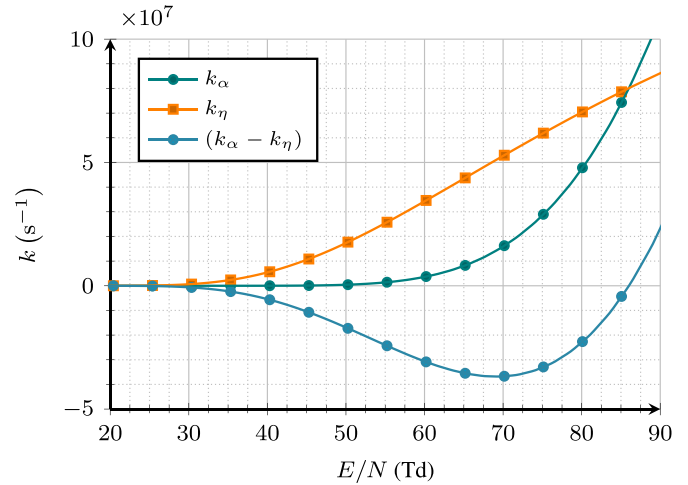


Figure 1. Ionization and attachment rate coefficients as functions of E/N at atmospheric pressure.

process is self-reinforcing. Suppose for a moment that some region in the streamer channel initially has an internal field $E/N = 50 \text{ Td}$. When dissociative attachment sets in, the field in the channel will start to increase as the conductivity is reduced. However, as we move rightwards in figure 1 from $E/N = 50 \text{ Td}$ the effective attachment rate increases further, which simply accelerates the rate of dissociative attachment and thus increases the field in the channel further. In recent calculations we showed that this mechanism is responsible for column glows and beads in so-called sprite discharges in the Earth atmosphere [18]. Malagón-Romero and Luque [19] also propose that the attachment instability is the reason why pilot systems [20] and space leaders [21] appear in meter-scale discharges, as they lead to optical emission and heating of localized segments of the streamer channel. However, it is not yet clear under which conditions the attachment instability begins to manifest since it requires a comparatively high initial electric field, well above the fields commonly observed in unperturbed streamer channels (at least for positive streamers in air). Our transport data nonetheless suggests that an attachment instability is also present in CO₂, which is of particular relevance to laboratory discharges as well as sprites in the Venusian atmosphere (which is mostly composed of CO₂).

2.4. Photoionization in CO₂

In contrast to the case of air where photoionization data is abundant and the primary states involved in the emission process have been identified, photoionization data for CO₂ is scarce. Photoionization in air primarily occurs due to a Penning effect where N₂ is first excited to the Carrol-Yoshino and Birge-Hopfield II bands, which have excitation energies higher than the ionization potential of O₂. The de-excitation pathways from excited N₂ are collisional relaxation (i.e. collisional quenching), and spontaneous emission. In the context of air, spontaneous emission rates are found in [22] (pre-dissociation is also a relevant relaxation mechanism for N₂).

When excited N_2 emits radiation through spontaneous emission it can ionize O_2 , and this supplies an efficient photoionization mechanism that produces free electrons. However, this mechanism relies on the availability of two molecular components with different ionization potentials, so there can be no pure effect like this in single-component gases like pure CO_2 . Photoionization in pure molecular gases must accordingly proceed first by formation of excited dissociation products, which is then followed by spontaneous emission of ionizing radiation. In CO_2 , this may occur due to emission from O_I , O_{II} , C_{II} , CO , and CO^+ [23]. Emission from these fragments, which form due to dissociative excitation of CO_2 , can thus ionize CO_2 which has an ionization potential corresponding to 90.5 nm radiation.

The emission cross sections for the dissociative fragments (O_I , O_{II} , C_{II} , CO , CO^+) that produce extreme ultraviolet (EUV) ionizing radiation below 90.5 nm are incomplete, which prevents us from using cross sections when deriving a photoionization model. Kanik *et al* [23] provide emission cross sections for 200 eV electrons and identify spectral peaks corresponding to emissions from O_I , O_{II} , C_{II} , CO , and CO^+ . For the 83.4 nm peak which corresponds to emission from O_{II} , the authors also present energy-resolved cross sections. The data in Kanik *et al* [23] is not available in tabulated form, but for an electron energy of 76.5 eV we may extract an approximate emission cross section of $1.78 \times 10^{-20} \text{ cm}^2$ (from figure 2 in [23]). The corresponding ionization cross section that we use at 76.5 eV energy is approximately $3.5 \times 10^{-16} \text{ cm}^2$, so the production of O_{II} emissions is considerably lower than the rate of electron impact ionization. Unfortunately, the precision in the figures by Kanik *et al* [23] makes it difficult to extract cross sections at lower electron energies and, furthermore, energy resolved cross sections are not available for the other EUV emissions.

The only available experiments that provide data for photoionization in CO_2 are due to Przybylski [24] who performed experiments at pressures of 1–3 Torr. Collisional quenching is most likely negligible at these pressures, and we have not been able to obtain data that describes the quenching rates of the involved EUV-emitting fragments. Even in air, quenching rates for the Carrol-Yoshino and Birge-Hopfield II bands of N_2 are not known individually (collisional de-excitation may occur at different rates for the two bands), but one may describe quenching by an approximate quenching pressure $p_q \sim 40 \text{ mbar}$. This leads to a correction in the photoionization level by $p_q/(p + p_q) \sim 0.04$ at 1 bar gas pressure, and this approach describes experiments with an acceptable level of accuracy [5].

The present situation for CO_2 is not ideal: appropriate energy-resolved emission cross sections at relevant electron energies are not available, and experimental data is only available for low-pressure CO_2 . The atomic fragments that emit the EUV radiation might be quenched differently, implying that collisional quenching does not only reduce the number of ionizing photons, but potentially also their spatial distribution. As we do not know of any data that provides an equivalent quenching pressure in CO_2 , we introduce a free parameter ν_q

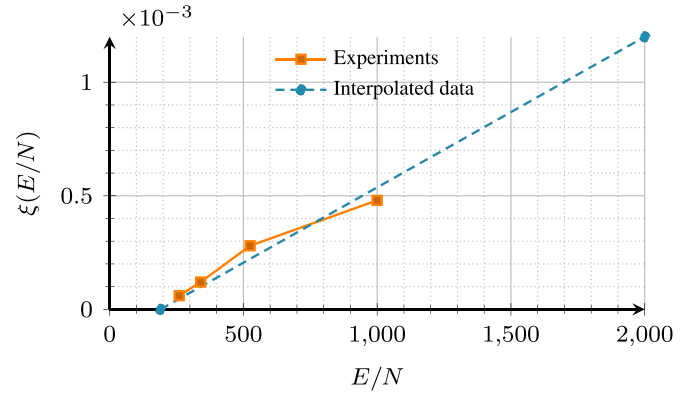


Figure 2. Coefficient $\xi(E/N)$, describing the number of ionizing photons produced per electron impact ionization event.

that adjusts the amount of photoionization in our simulations, which is to be interpreted as follows: the quenching behavior of the EUV-emitting fragments (e.g. O_I) following impact dissociation of CO_2 obeys

$$\partial_t O_I = -\frac{O_I}{\tau} - (k_q N) O_I, \quad (6)$$

where τ is the radiative lifetime and $k_q N$ is the quenching rate. Quenching occurs due to collisions between O_I and neutral CO_2 molecules, so the quenching rate grows linearly with neutral density N . The number of photoemission events per de-excitation of O_I is then $\frac{\tau^{-1}}{\tau^{-1} + k_q N}$, and as N is proportional to pressure ($p = Nk_B T$), collisional quenching can reduce the amount of photoionization at higher pressures. Similar relations could be formulated for the other fragments, but as none of the corresponding rate constants (τ^{-1} and k_q) are known, we lump this factor into a single term ν_q .

The photon production rate k_γ in our calculations is then calculated as

$$k_\gamma(\nu_q) = \nu_q \xi(E/N) k_\alpha, \quad (7)$$

where $\nu_q \leq 1$ phenomenologically describes a reduction in the production of ionizing photons due to collisional quenching, and $\xi(E/N)$ is a field-dependent proportionality factor that describes the number of photoionization events per electron impact ionization event as originally measured by Przybylski [24]. For air, $\xi(E/N)$ is approximately 0.06, while for CO_2 the reported value is at least one order of magnitude smaller. We have presented this data in figure 2 versus E/N . The experimental data is limited to $E/N \in [220 \text{ Td}, 1000 \text{ Td}]$, so we linearly extrapolate the data as indicated in the figure. This extrapolation is done because we observe that very high fields develop in computer simulations with low values of ν_q , while emission cross sections generally peak at around 200 eV [23].

Unfortunately, the factor ν_q is not known with desired accuracy, and the experiments by Przybylski [24] also contain substantial uncertainties. For example, it is not known if the reported data Przybylski [24] represent total photoionization or photoionization per steradian Przybylski [2]. In the

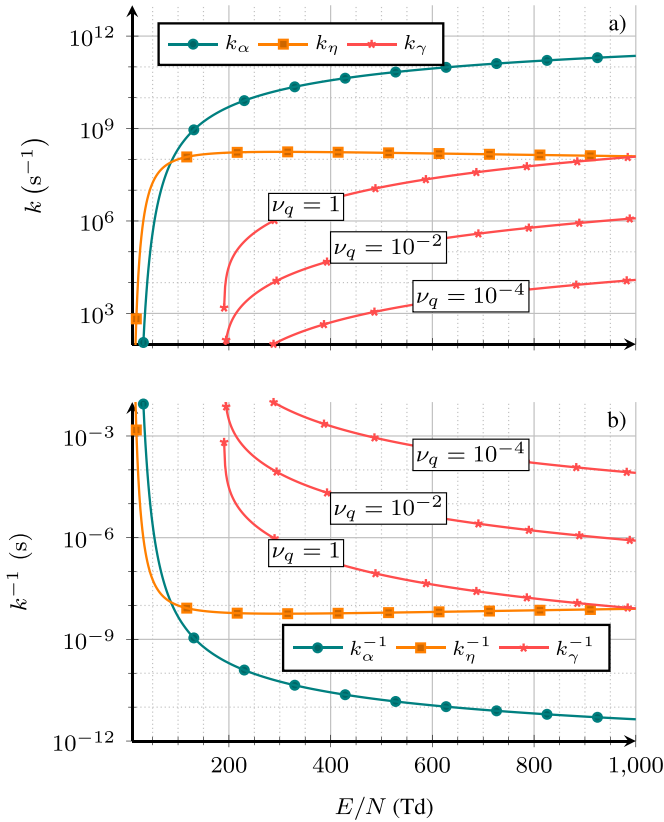


Figure 3. (a) Ionization, attachment, and photon production rates for various quenching efficiencies ν_q . (b) Inverse rates (i.e. lifetimes).

latter case, the photoionization efficiency $\xi(E/N)$ that we use in this paper needs to be multiplied by a factor of 4π . Due to these circumstances, we choose a simple approach in which we consider $\nu_q = 1$ as a baseline case. This is the upper limit of the photoionization level where no quenching takes place, which can e.g. happen if the radiative lifetimes of the emitting fragments are very short. Note that due to the uncertainties in the experiments by Przybylski [24], $\nu_q = 1$ potentially already underestimates the photoionization level by a factor of 4π .

Figure 3(a) shows the rates k_α , k_η , and $k_\gamma(\nu_q)$ for $\nu_q = 10^{-4}$, 10^{-2} and 1 as functions of the reduced electric field E/N . We also include the inverse rates (i.e. lifetimes) of these reactions in figure 3(b). The reaction lifetimes describe the average time before an electron triggers the reaction, and we can see that each electron generates one impact ionization collision every $k_\alpha^{-1} \sim 10$ ps at $E/N \sim 600$ Td. However, the lifetime $k_\gamma(\nu_q = 1)$ is approximately 10 ns at the same field strength, and photoionization events are thus rare compared to ionization events.

CO_2 absorbs quite strongly in the 83–89 nm spectral range, where the pressure-reduced mean absorption coefficient is between $\kappa_{\min}/p = 0.34/(\text{cm Torr})$ and $\kappa_{\max}/p = 2.2/(\text{cm Torr})$ [2]. At atmospheric pressure this corresponds to mean photon absorption lengths between $6 \mu\text{m}$ and $38 \mu\text{m}$. This is shorter than in air, where mean absorption lengths are between $30 \mu\text{m}$ and 2 mm at atmospheric pressure.

When computational photons are generated in our simulations, their mean absorption coefficient is computed as

$$\kappa = \kappa_{\min} \left(\frac{\kappa_{\max}}{\kappa_{\min}} \right)^U, \quad (8)$$

where U is a random number sampled from a uniform distribution on the interval $[0, 1]$, and κ_{\min} and κ_{\max} are as given above. Only a few photons are generated per time step and cell. A rough estimate may be obtained from figure 3(a) with $E/N = 600$ Td, where $k_\gamma \sim 2.75 \times 10^5 \text{ s}^{-1}$, while typical plasma densities n_e at streamer tips are $10^{18} - 10^{20} \text{ m}^{-3}$. Time steps are typically $\Delta t \sim k_\alpha^{-1} \approx 10$ ps and grid cell volumes in the streamer head are $\Delta V \sim 8 \times 10^{-18} \text{ m}^3$. The mean number of photons generated per cell and time step is roughly $k_\gamma n_e \Delta t \Delta V$ which evaluates to between 2×10^{-5} and 2×10^{-3} photons on average. Note that this estimate is per grid cell; the total number of ionizing photons emitted from a streamer head will be substantially higher. We point out that the computational photons in our calculations correspond to physical photons, so there is no artificial elevation of discrete particle noise due to photoionization.

2.5. Simulation conditions

Our simulations are performed in the protrusion-plane geometry shown in figure 4, which has dimensions of $12 \text{ cm} \times 3 \text{ cm} \times 12 \text{ cm}$. The discharges initiate at the tip of a 5 mm long electrode that protrudes downwards along the z -axis. The gap distance between the electrode and the ground plane is 25 mm. The protrusion radius is 1 mm, and narrows along a conical section with a full opening angle of 30 degrees and a tip radius of $200 \mu\text{m}$. All calculations are performed for a standard atmosphere (i.e. pressure $p = 101325 \text{ Pa}$ and temperature $T = 300 \text{ K}$).

For the electric potential Φ we use homogeneous Neumann boundary conditions ($\partial_n \Phi = 0$) on the side faces and Dirichlet boundary conditions on the top and bottom faces. The lower face is always grounded ($\Phi = 0$) while the upper face and the protrusion are always at live voltage $\Phi = V$ where V is a constant applied voltage which is varied in our computer simulations. We also define the average electric field between the electrode and the ground plane as

$$E_{\text{avg}} = \frac{V}{L}, \quad (9)$$

where $L = 25 \text{ mm}$. The baseline quenching efficiency that we use in our simulations is $\nu_q = 1$, but we vary this in sections 3.2 and 3.4.

All simulations begin by sampling 100 physical electrons with random positions inside a $200 \mu\text{m}$ radius sphere centered at the electrode tip. Initial electrons whose positions end up inside the electrode are discarded before the simulation begins. The initializing particles are unique to each simulation.

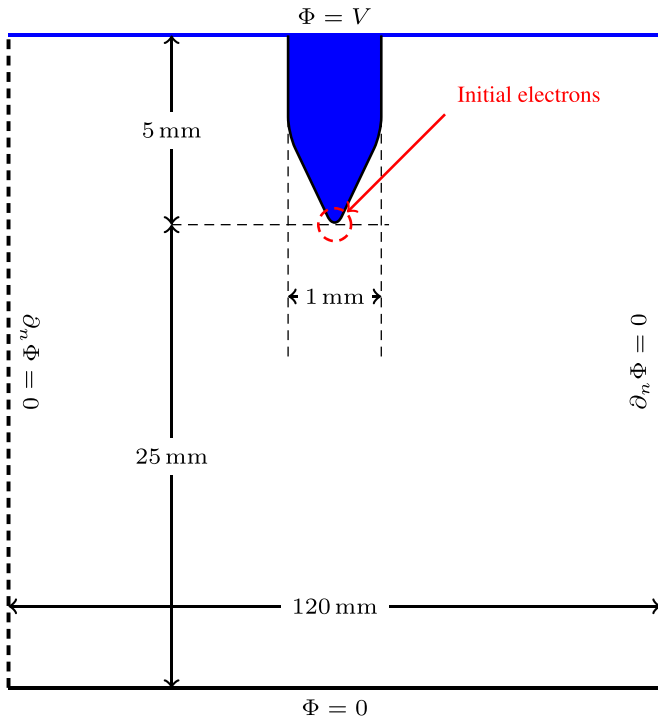


Figure 4. Sketch (not to scale) of the computational domain with electrostatic boundary conditions. The rounding radius at the needle tip is $200\ \mu\text{m}$ and the full opening angle of the conical section on the electrode is 30 degrees.

2.6. Numerical discretization

We use the chombo-discharge code [12] for performing our computer simulations. As the full discretization and implementation of the model are quite elaborate, we only discuss the basic features here.

In time, we use a Godunov operator splitting between the plasma transport and reaction steps, where the transport step is semi-implicitly coupled to the electric field (see [25] for another type semi-implicit coupling for fluid discretizations). After the transport step we resolve the reactions in each grid cell using a KMC algorithm. Unlike the deterministic reaction rate equation, the KMC algorithm is fully stochastic and operates with the number of particles in each grid cell rather than the particle densities. Complete details are given in [11]. Constant time steps $\Delta t = 10\ \text{ps}$ are used in our simulations.

In space, we use an adaptive Cartesian grid with an embedded boundary (EB) formalism for solid boundaries. EB discretization, also known as cut-cell discretization, is a special form of boundary discretization and brings substantial complexity into the discretization schemes (e.g. see [26]). In return it permits use of almost regular Cartesian data structures, and allows us to apply adaptive mesh refinement in the presence of complex geometries with comparatively low numerical overhead. Special handling of discretization routines is introduced at cut-cell and refinement boundaries. For example, we always enforce flux matching for the Poisson equation [27], and particles are deposited using custom deposition methods near refinement boundaries [11].

We discretize the 3D domain using $256 \times 64 \times 256$ cells and add 9 levels of grid refinement which are dynamically adapted as simulations proceed. The refinement factor between adjacent grid levels is always 2, so the finest representable grid cell in our simulation is $\Delta x \approx 0.91\ \mu\text{m}$. Grid cells are refined every 5 time steps (i.e. every 50 ps) if

$$\bar{\alpha}\Delta x \geq 1, \quad (10)$$

where $\bar{\alpha}$ is the effective Townsend ionization coefficient. Likewise, grid cells are coarsened if

$$\bar{\alpha}\Delta x \leq 0.1 \quad (11)$$

and Δx was no larger than $8\ \mu\text{m}$.

The $\hat{\text{Ito}}$ -KMC model we use is a particle-based model for the electrons, and particle re-balancing is required since the number of physical electrons at the streamer tips grows exponentially in time. Particle merging and splitting is done following our previous approach discussed in [11] where bounding volume hierarchies are used for group partitioning of particles within a grid cell. The algorithm is run at every time step, and ensures that computational particle weights within a grid cell differ by at most one physical particle. In all simulations we limited the maximum number of computational particles to 32.

Our time step is quite large compared to conventional time steps used for fluid models, and can lead to numerical errors that affect the accuracy of our results. To determine how close our calculations are to numerical convergence, we have presented a sensitivity study in appendix, where we use smaller time steps under otherwise identical simulation conditions. In summary, these auxiliary calculations show that our usage of a large time step lead to slight numerical underresolution where the streamer velocities are underestimated by about 25%–30%, while streamer radii, electron densities, and electric fields at the streamer tips are otherwise unaffected by the time step selection.

The calculations in this paper were performed on 8–80 nodes on the Betsy supercomputer, where each node consists of dual AMD EPYC 7742 CPUs. Each node has 2×64 CPU cores, corresponding to a total of 1024–10240 CPU cores for the various simulations. Meshes ranged up to 2.5×10^9 grid cells and 10^{10} computational particles, with various simulations completing in 0.5–5 days.

3. Results

3.1. Negative streamers versus voltage

In this section we present results for the evolution of negative streamers for voltages $V \in [-25\ \text{kV}, -30\ \text{kV}, -35\ \text{kV}]$. These voltages corresponds to average electric fields of $1\ \text{kV}\ \text{mm}^{-1}$, $1.2\ \text{kV}\ \text{mm}^{-1}$, and $1.4\ \text{kV}\ \text{mm}^{-1}$. We performed a single 3D simulation for each voltage, and present the results in figure 5.

3.1.1. Streamer propagation field. The top row in figure 5 shows that a negative streamer started at a voltage of $V = -25\ \text{kV}$, but the discharge did not propagate very far during

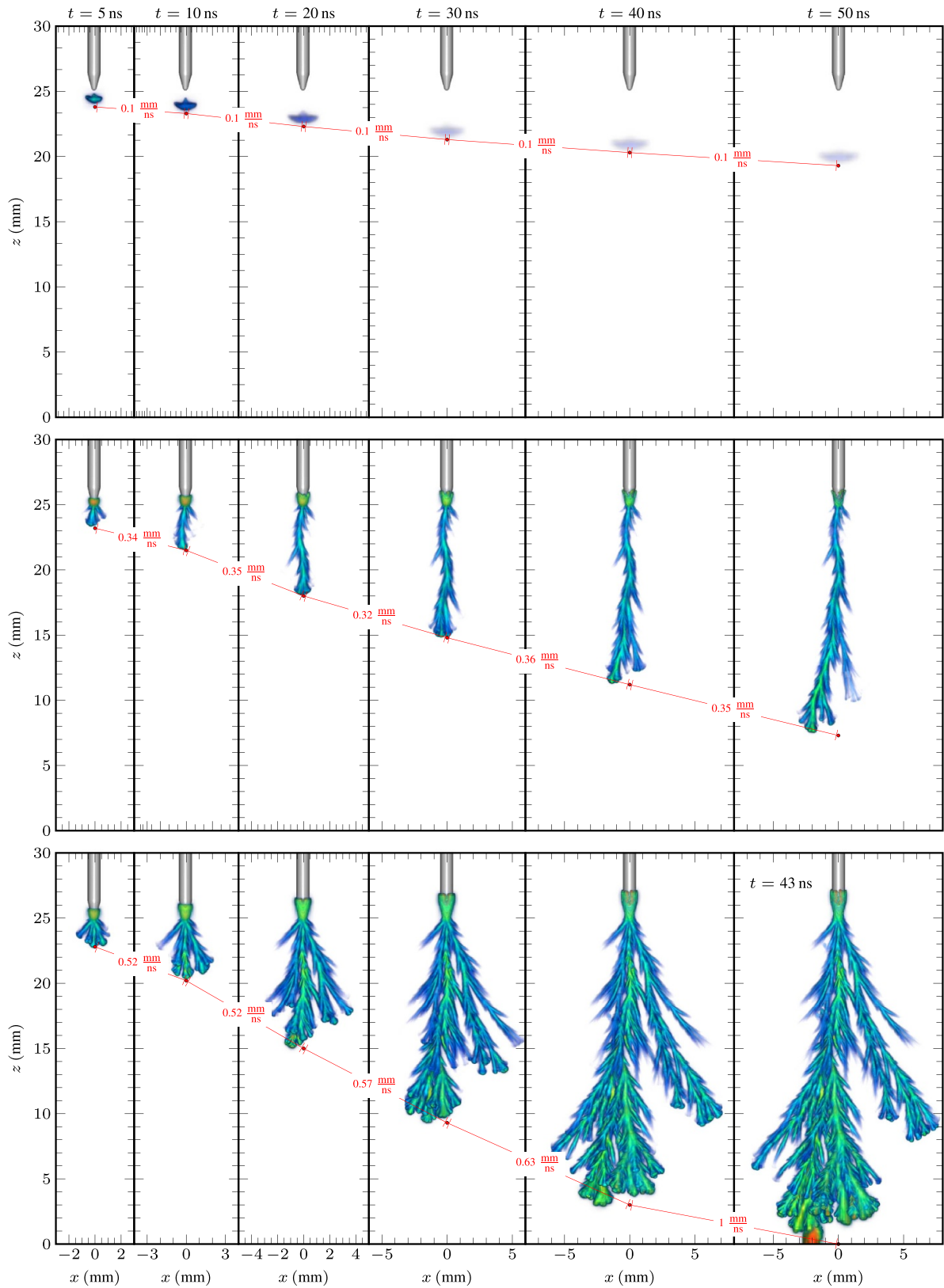


Figure 5. Negative streamer evolution using various applied voltages. Top row: $V = -25 \text{ kV}$ ($E_{\text{avg}} = 1 \text{ kV mm}^{-1}$). Middle row: $V = -30 \text{ kV}$ ($E_{\text{avg}} = 1.2 \text{ kV mm}^{-1}$). Bottom row: $V = -35 \text{ kV}$ ($E_{\text{avg}} = 1.4 \text{ kV mm}^{-1}$), where the final frame shows a snapshot when the streamer connects to the ground plane after $t = 43 \text{ ns}$. The dashed lines shows the average vertical velocities (between the indicated markers in each figure).

the 50 ns simulation time. The streamer was not electrically connected (with plasma) to the cathode either, and propagated as a diffuse cloud of electrons that gradually broadened and weakened with propagation distance. While we did not run the simulation further, we expect that the discharge would eventually fade out and decay. The middle row in figure 5 shows negative streamers at a voltage of $V = -30\text{ kV}$, corresponding to an average electric field of $E_{\text{avg}} = 1.2\text{ kV mm}^{-1}$. The streamer is characterized by a main branch with numerous side branches, many of which stagnate early and do not propagate further. This streamer did not cross the discharge gap in the course of the simulation, although we expect that it would have if the simulation was run further. Finally, the bottom row shows the streamer development with an applied voltage of $V = -35\text{ kV mm}^{-1}$, corresponding to $E_{\text{avg}} = 1.4\text{ kV mm}^{-1}$. The discharge consists of multiple branches that form a broad discharge tree approximately 15 mm wide, and crossed the discharge gap in 43 ns.

From the results we conclude that negative streamers in our simulations propagate if the average electric field is $E_{\text{avg}} \in 1\text{--}1.2\text{ kV mm}^{-1}$. Incidentally, Seeger *et al* [7] report that the negative streamer stability field derived from their experiments is $(11 \pm 2)\text{ V (mPa)}^{-1}$, which translates to $(11 \pm 2)\text{ kV mm}^{-1}$ at 1 bar gas pressure. We thus find quantitative agreement between experiments [7] and our observed propagation fields.

3.1.2. Velocity. In the computer simulations we observe that the front velocity of the discharge is voltage dependent, and that it varies during the discharge evolution. We have indicated the velocities in figure 5, which are calculated by estimating how far the vertical front position of the discharge has moved between the frames. At the lowest voltage ($V = -25\text{ kV}$) the discharge propagated with an average velocity of 0.1 mm ns^{-1} , but as we mentioned above the discharge does not represent a propagating streamer. For $V = -30\text{ kV}$ the observed velocity remained fairly constant throughout the propagation phase, with an approximate value of $v = 0.34\text{--}0.36\text{ mm ns}^{-1}$. The bottom row in figure 5 shows that at the highest simulated voltage $V = -35\text{ kV}$ the front velocity varied a great deal throughout the streamer development. For $t < 20\text{ ns}$ the streamer velocity was approximately 0.52 mm ns^{-1} , which increased to approximately 1 mm ns^{-1} as the streamer approach the ground plane.

Seeger *et al* [7] have measured approximate streamer velocities in CO_2 , using a single PMT for estimating the propagation time of the streamer and an image intensified (ICCD) camera for measuring the streamer length. The results for negative streamers were obtained for a field distribution slightly different from ours, and the authors report negative streamer velocities in the range of $0.2\text{--}0.6\text{ mm/ns}$ at 1 bar gas pressure. We also point out that this velocity interval represents average streamer velocities rather than instantaneous velocities. Our simulation results nonetheless agree quite well with the experimental values, despite the fact that the experimentally estimated streamer velocities contain uncertainties due to the measurement method.

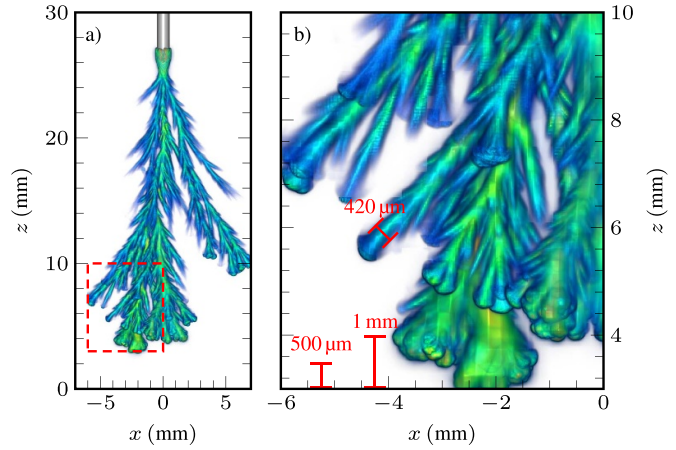


Figure 6. Determination of the minimum negative streamer radius for an applied voltage $V = -35\text{ kV}$ after $t = 40\text{ ns}$, using the plasma density n_e as a proxy for the electrodynamic radius. (a) Full view, showing plasma densities $n_e \geq 10^{18}\text{ m}^{-3}$. (b) Inset of the indicated region in (a).

3.1.3. Radius. Figure 5 shows that the negative streamers branch frequently, and many of the branches also stagnate, which makes it difficult to extract a single streamer radius in our calculations. Since negative streamers can broaden quite efficiently, a range of streamer radii can probably be observed also in experiments. In experiments, only the optical radius of the streamers are available, and Seeger *et al* [7] report experimentally obtained negative streamer radii as $(25 \pm 3)\text{ mPa}$, which translates to $250\text{ }\mu\text{m}$ at atmospheric pressure. This was the smallest radius observed in the experiments [7]. Our simulations do not model optical emission in the CO_2 plasma, so only the electrodynamic radius is available. These measures can differ substantially. For positive streamers in air it is estimated that the electrodynamic radius is twice that of the optical radius [28], but no corresponding relation has been reported for negative streamers.

Figure 6 shows the plasma density for the simulation with $V = -35\text{ kV}$ after $t = 40\text{ ns}$. In figure 6(b) we have also included various length indicators, as well as the diameter of a specific branch which initially propagated but later stagnated. Examining the various branches in the figure we find that the smallest electrodynamic diameter of the filaments is at least $420\text{ }\mu\text{m}$, in good agreement with experimentally reported values [7]. We point out that this radius is obtained for a branch that propagated only over a short distance, possibly because this branch was screened by the negative streamer front. There is thus some uncertainty in the determination of the smallest negative streamer diameter in our simulations. Nonetheless, similar diameters (at least $420\text{ }\mu\text{m}$) are also found for $V = -30\text{ kV}$ in figure 5.

3.1.4. Field distribution. In order to obtain an estimate for the range of electric fields that occur on negative streamer tips, figure 7 shows an isosurface $n_e = 10^{18}\text{ m}^{-3}$ of the plasma after $t = 30\text{ ns}$ for the simulation with $V = -35\text{ kV}$. Depending

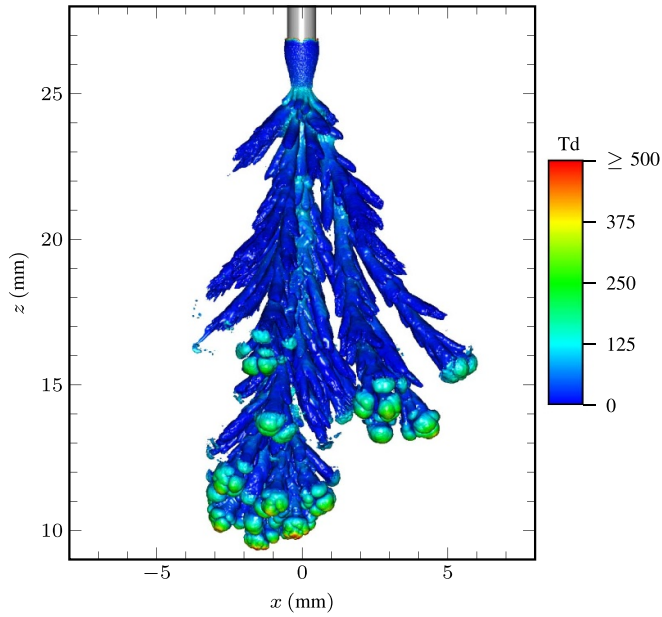


Figure 7. Isosurface $n_e = 10^{18} \text{ m}^{-3}$ for $V = -35 \text{ kV}$ after $t = 30 \text{ ns}$. The surface is colored by the reduced electric field E/N .

on the radius and position of the negative streamer tips, we find that the electric field at the negative streamer tips is 200–520 Td (note that figure 7 uses a truncated color range). For comparison, reported electric fields for negative streamers in air are approximately 300 Td [29].

Next, we examine the evolution of the electric field in the streamer channels. Figure 8 shows snapshots of electric field lines at various time instants for the simulation with $V = -35 \text{ kV}$. Field lines are pruned from the plot if the electron density is $n_e < 10^{18} \text{ m}^{-3}$ so that all field lines in figure 8 pass through the plasma. The field lines are colored by E/N , and transparency channels are added such that field lines with $E/N \geq 80 \text{ Td}$ are opaque and field lines with $E/N = 0 \text{ Td}$ are completely transparent. Figure 8 shows that localized regions in the streamer channel with initially low electric fields later develop comparatively high fields $E/N > 70 \text{ Td}$. We have indicated one of these regions by a dashed circle in figure 8, but other regions can also be identified. The field enhancement in the channels is caused by dissociative attachment which reduces the conductivity of the channel, as discussed in section 2. The conductivity reduction is then compensated by an increased electric field, similar to how the attachment instability operates in air [16].

3.1.5. Cathode sheath. Negative streamers propagate away from the cathode and leave behind positive space charge composed of positive ions, which can lead to a sheath immediately outside of the cathode surface. The sheath is electron-depleted because the electrons in it propagate away from the cathode (and thus out of the sheath). Analogous sheaths also exist for positive streamers propagating over dielectric surfaces [12, 30, 31]. Unfortunately, we can not study the details in the sheath with desired accuracy because of the inherent limitations of

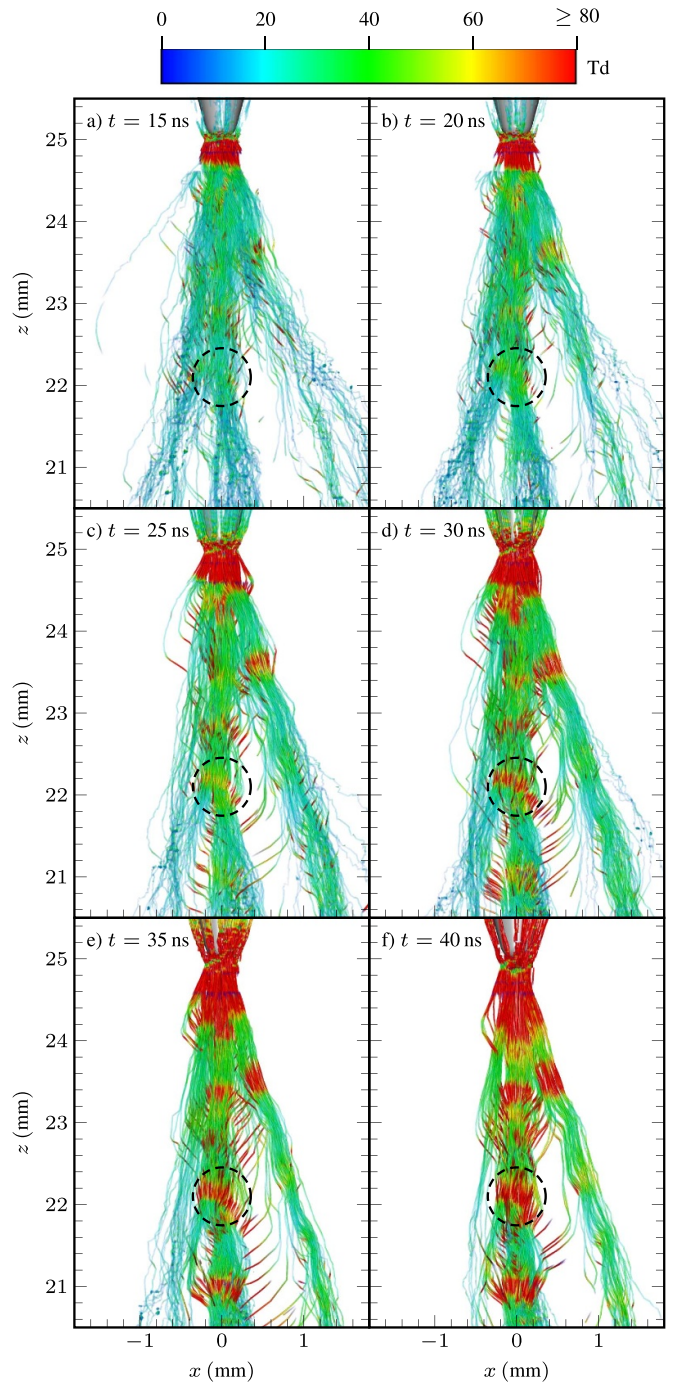


Figure 8. Field lines in the plasma colored by electric field (in units of Td, for $V = -35 \text{ kV}$ applied voltage). The color range is truncated to $E/N \in 0-80 \text{ Td}$ with alpha channels that reduce the opacity of the field lines with lower E/N .

the LFA. Physically, secondary electrons that appear in the sheath are due to photoionization, cathode emission, or electron impact ionization. The secondary electrons arising from these processes are low-energy electrons that do not generate further impact ionization until they have been sufficiently accelerated to above-ionization energies. But in LFA-based models these electrons are always born with artificially high

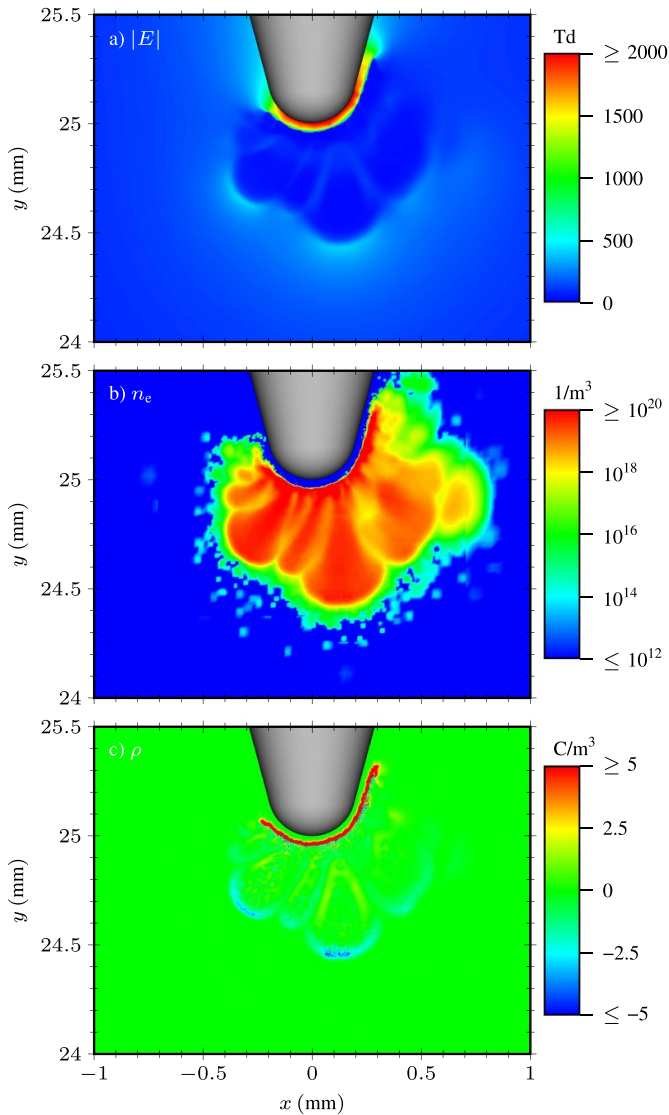


Figure 9. Cathode sheath region details at $t = 2.5$ ns. The data in each figure shows a slice through the z -plane in the simulation with $\nu_q = 1$, $V = -35$ kV. (a) Electric field magnitude. (b) Electron density. (c) Space charge density.

energies, parametrically given as a function of E/N . In our model, photoelectrons that appear in the sheath can thus immediately ionize the gas, which is non-physical since their true energy is $\mathcal{O}(1 \text{ eV})$. Our model therefore predicts an artificially high level of impact ionization in the sheath region, and we can thus only make a qualitative assessment of the sheath features (such as its thickness).

Figure 9 shows some details of the cathode sheath region for the computer simulation with $\nu_q = 1$, $V = -35$ kV, where we include slice plots of the electric field magnitude, the electron density, and the space charge density. From the figure we find a sheath thickness of approximately $50 \mu\text{m}$, and fields that range up to 2000 Td . Figure 9(c) shows the reason why this high field region appears, which is due to CO_2^+ ions that have accumulated just outside the cathode surface. Since the cathode surface is charged negatively and the space charge is positive, there is a corresponding high field region between these

two features. This field will not persist indefinitely because as the ions move slowly towards the cathode, the space charge layer is gradually absorbed by the cathode and the field in the sheath will correspondingly decrease. We have not shown this process in detail but point out that it occurs on a comparatively long time scale (tens to hundreds of nanoseconds) due to the comparatively low ion mobility. For sheaths along dielectric surfaces, this can lead to charge saturation, as demonstrated by Meyer *et al* [32].

3.2. Negative streamers without photoionization

Few publications have addressed the role of photoionization in negative streamers. Most of the available results are for air and with continuum approximations for the photons [33, 34]. Starikovskiy and Aleksandrov [34] provide a qualitative explanation on the role of photoionization for negative streamers: seed electrons that appear ahead of negative streamers turn into avalanches that propagate outwards from the streamer tip, which facilitates further expansion of the streamer head. When the negative streamer head expands, field enhancement and thus impact ionization at the streamer tip decreases, which leads to a slower streamer. Similar conclusions were reached by Luque *et al* [29], who also point out that this broadening can also lead to negative streamer decay (similar to figure 5 for $V = -25$ kV).

It is important to note that the above cited results all use continuum approximations for photoionization, which is not a valid approximation for our conditions. The role of discrete photoionization for positive streamers in air has been reported [3, 4], and the studies show that positive streamer morphologies depend sensitively on the photoionization parameters. Analogous studies for negative streamers in air have not yet been reported. However, since photoionization can provide seed electrons ahead of negative streamers in precisely the same way as for positive streamers, photoionization might also play a role in the branching of negative streamers.

Figure 10 shows the plasma density for a case where photoionization is fully turned off ($\nu_q = 0$). The applied voltage is $V = -35$ kV, i.e. corresponding to the bottom row in figure 5, which is included for the sake of comparison. Without photoionization, the negative streamer propagates much slower than its photoionization-enabled counterpart, and it eventually also decays.

The computer simulations also show that the cathode sheath dynamics are affected by photoionization. Figure 10 shows that the cathode is partially covered by plasma when photoionization is enabled ($\nu_q = 1$). This plasma is a positive streamer that propagates upwards along the cathode, and it leaves behind a positive space charge layer outside the cathode (as seen in figure 9). The sheath is thus affected by the appearance of seed electrons in the cathode region, in particular seed electrons that appear in the cathode fall since these electrons initiate new avalanches that leave behind additional space charge. As this process cascades, it leads to inception of a positive streamer that propagates towards and finally along the cathode surface. Without photoionization, the

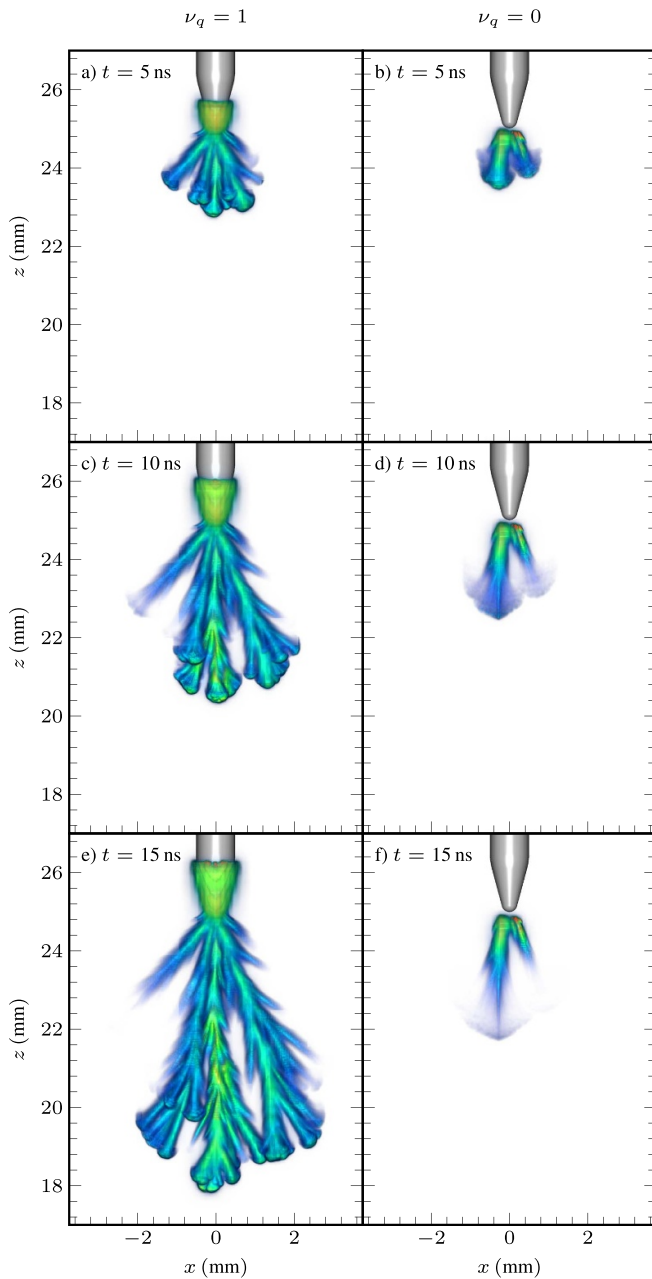


Figure 10. Evolution of a negative streamer with $V = -35$ kV with photoionization ($\nu_q = 1$) and without photoionization ($\nu_q = 0$).

necessary seed electrons that are required in order to facilitate the positive streamer no longer appear. The upwards propagating positive streamer does not manifest without this source of electrons, and this reduces the intensity of the space charge layer close to the cathode and also the field in the cathode sheath.

While figure 10 shows that photoionization is important for the negative streamer evolution, it does not answer whether or not this is due to conditions at the negative streamer tip, or due to absence of the upwards positive streamer. The positive streamer feeds a current into the system, and consequently it affects the potential distribution and field enhancement of the negative streamer head.

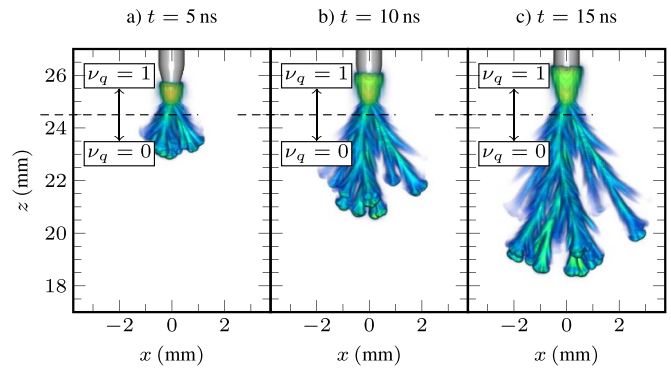


Figure 11. Evolution of a negative streamer with $V = -35$ kV, using $\nu_q = 1$ for $z > 24.5$ mm and $\nu_q = 0$ elsewhere.

In order to determine whether or not the decay of the negative streamer seen in figure 10 is due to lack of photoionization at the negative streamer tip or absence of a positive cathode-directed streamer, we run another computer simulation where generation of ionizing photons is turned off in all regions where $z < 24.5$ mm. This is equivalent to turning off photoionization for the propagating negative streamer, but maintaining photoionization for the upwards positive streamer that propagates along the cathode surface. Figure 11 shows the results for this simulation, and should be contrasted with the left and right columns in figure 10. The evolution of the negative streamer for this case is qualitatively similar to the left column of figure 10 where photoionization was enabled everywhere. Consequently, photoionization at negative streamer tips in CO_2 does not appear to play a major role in the streamer evolution. However, appropriate coupling to the cathode still requires inclusion of photoionization; inception of the upwards positive streamer in the sheath region ultimately leads to a voltage drop across the sheath, which increases field enhancement at the negative streamer tip and thus facilitates its propagation. In this paper we have not modeled secondary electron emission from the cathode, but conjecture that a similar behavior will manifest in this case since cathode emission can also lead to free electrons in the cathode sheath region. Qualitatively, the free electrons that enable ionization in the emerging sheath region will then be due to cathode emission (e.g. from positive ion impact) rather than photoionization.

3.3. Positive streamers versus voltage

In this section we consider propagation of positive streamers for voltages $V \in [20 \text{ kV}, 25 \text{ kV}, 30 \text{ kV}, 35 \text{ kV}]$. We perform the study in the same way as we did for negative streamers: a single computer simulation is performed for each voltage application, and we extract velocities, radii, and field distributions. The evolution of the corresponding discharges is shown in figure 12.

3.3.1. Streamer propagation field. The top row in figure 12 shows the evolution of positive streamers in CO_2 at $V = 25$ kV, which corresponds to an average electric field of

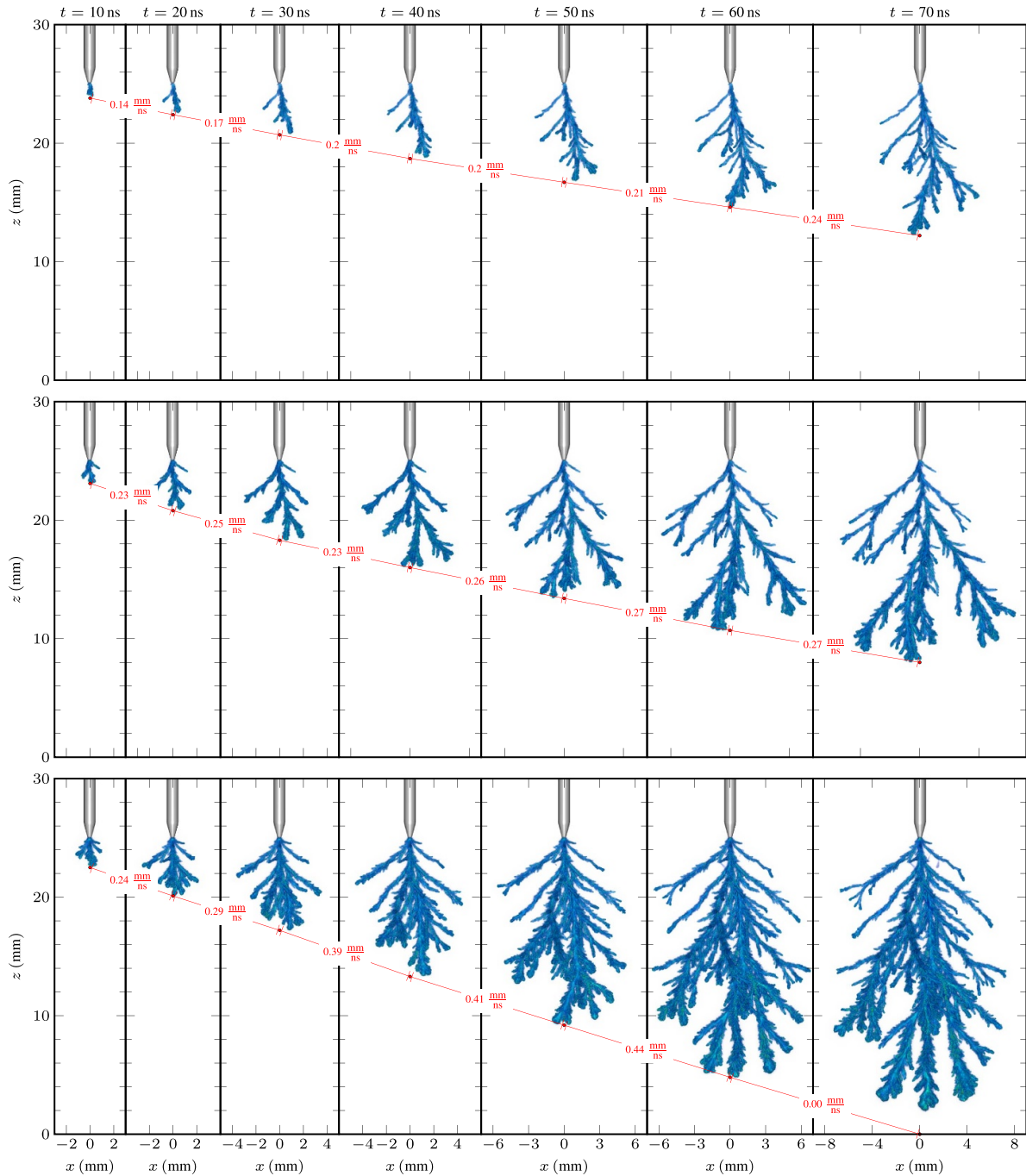


Figure 12. Positive streamer evolution with various applied voltages. Top row: $V = 25 \text{ kV}$ ($E_{\text{avg}} = 1 \text{ kV mm}^{-1}$). Middle row: $V = 30 \text{ kV}$ ($E_{\text{avg}} = 1.2 \text{ kV mm}^{-1}$). Bottom row: $V = 35 \text{ kV}$ ($E_{\text{avg}} = 1.4 \text{ kV mm}^{-1}$). The final frame shows the plasma at $t = 66.5 \text{ ns}$, immediately before the streamer connected to the ground plane. The dashed lines shows the average vertical velocities (between the indicated markers in each figure).

$E_{\text{avg}} = 1 \text{ kV mm}^{-1}$. We did not include the simulation with $V = 20 \text{ kV}$ ($E_{\text{avg}} = 0.8 \text{ kV mm}^{-1}$) in figure 12 because a positive streamer failed to develop at this voltage. The middle row in figure 12 shows the evolution for $V = 30 \text{ kV}$ ($E_{\text{avg}} = 1.2 \text{ kV mm}^{-1}$) and the bottom row shows the evolution with $V = 35 \text{ kV}$ ($E_{\text{avg}} = 1.4 \text{ kV mm}^{-1}$). Qualitatively, we observe that with increasing voltage the streamers evolve into broader and faster discharge trees. The discharges also grow much more irregularly than for negative polarity (see figure 5).

Our baseline simulations show that positive streamers develop at $V = 25 \text{ kV}$ but not $V = 20 \text{ kV}$, indicating that the streamer propagation field in our calculations is $0.8\text{--}1 \text{ kV mm}^{-1}$. This is, in fact, substantially lower than what is observed in experiments where the reported streamer propagation field at 1 bar is approximately 1.3 kV mm^{-1} [7]. For positive streamers, our calculations of the streamer propagation field therefore contain an error of about 30%–50%.

3.3.2. Velocity. Like we found with negative streamers, figure 12 shows that the front velocity of the discharge depends on the applied voltage and also that it varies during the discharge evolution. With $V = 25$ kV the discharge propagated with an average velocity of approximately 0.2 mm ns^{-1} , which is lower than the slowest negative streamer we observed ($V = -30$ kV). For $V = 30$ kV the observed velocity increased to approximately $0.23\text{--}0.27 \text{ mm ns}^{-1}$, while for $V = 35$ kV the velocity was $0.24\text{--}0.44 \text{ mm ns}^{-1}$. Our simulations show that positive streamers propagate slower than negative streamers, in agreement with experiments [7]. For comparison, the corresponding average velocities deduced from experiments are $0.1\text{--}0.5 \text{ mm ns}^{-1}$, so our velocity calculations are in comparatively good agreement. Finally, we make a qualitative observation regarding the streamer velocities. For both negative and positive streamers the thickest streamer branches are always found at the front, which indicates that thicker branches propagate faster. This feature is similar to the behavior in air, where the streamer velocity v and diameter d obey an empirical relation $v \propto d^2$ [6].

3.3.3. Radius. Figure 12 shows that positive streamers in CO_2 can develop into tree structures that have a distribution of radii, i.e. there is no unique streamer radius. As we did for negative streamers, we only extract the radius for streamer filaments that do not branch, using regions where $n_e \geq 10^{18} \text{ m}^{-3}$ as a proxy for the electrodynamic radius. Figure 13 shows the simulation data for $V = 25$ kV after $t = 50$ ns. Various length indicators are included, as well as the diameter of a specific branch that did not branch, but whose path fluctuated. From this branch we extract an approximate radius of $140 \mu\text{m}$. This agrees quite well with the experiments by Seeger *et al* [7] who report that the optical radius of positive streamers is at least $(13.4 \pm 3.0) \text{ mPa}$, which translates to $130 \mu\text{m}$ at atmospheric pressure. In atmospheric pressure air, the minimum (optical) radius for positive streamers has been reported to be around $100 \mu\text{m}$ [6, 35]. The corresponding velocities for such streamers were 0.1 mm ns^{-1} , so that radii and velocities for positive streamers in air and CO_2 are quite similar at atmospheric pressure.

3.3.4. Field distribution. As we discussed in section 3.1 we found that on longer timescales the field in negative streamer channels gradually increase due to an attachment instability that reduces the channel conductivity and hence increases the field in the channel. We have not found any corresponding field increase in positive streamer channels, which suggests that the field is too low for the attachment instability to manifest at the positive streamer evolution time scale. Figure 14 shows the field distribution along field lines in the streamer channels, i.e. regions where $n_e \geq 10^{18} \text{ m}^{-3}$. In positive streamer channels we find that the internal electric field is $10\text{--}20 \text{ Td}$. For comparison, this is the same value as positive streamers in atmospheric air, which is usually reported as being around 20 Td [29].

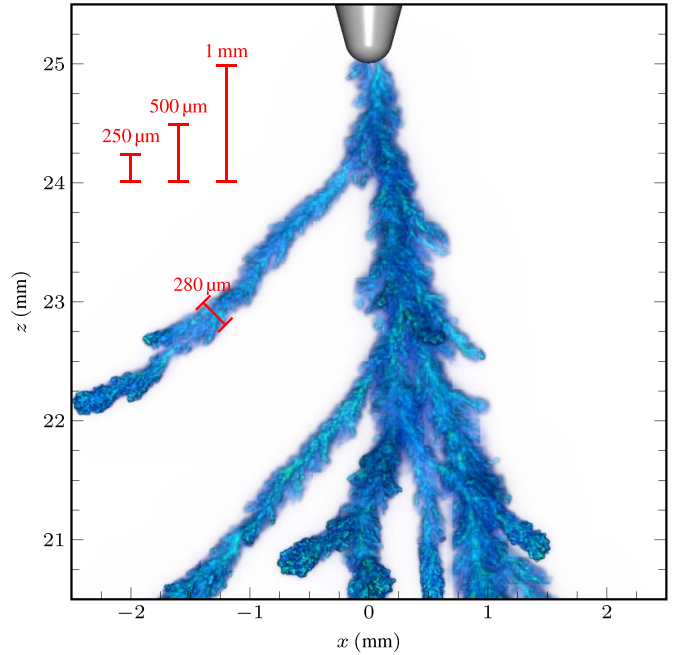


Figure 13. Determination of the minimum positive streamer radius for an applied voltage $V = 25$ kV after $t = 50$ ns, using the plasma density n_e as a proxy for the electrodynamic radius.

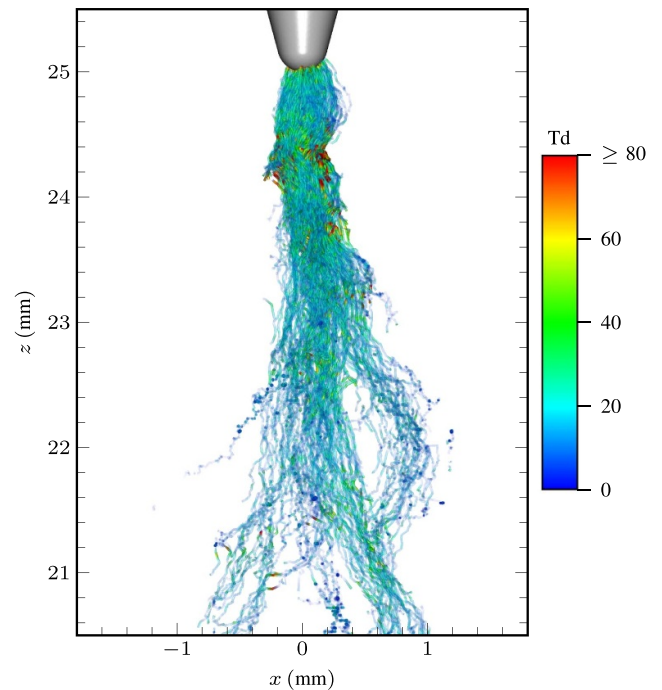


Figure 14. Field lines in the plasma colored by electric field (in units of Td, for $V = 35$ kV applied voltage after $t = 39$ ns. The color range is truncated to $E/N \in 0\text{--}80 \text{ Td}$ with alpha channels that reduce the opacity of the field lines with lower E/N .

Figure 15 shows an isosurface $n_e = 10^{18} \text{ m}^{-3}$ for the simulation with $V = 30$ kV after $t = 56$ ns. The isosurface is colored by the reduced electric field E/N , and shows the reduced

electric field at positive streamer tips. Typical fields are 600–900 Td, but we point out that the positive streamer fronts are quite irregular with local enhancements of the field at their tips, as can be seen in figure 15(b) which shows a closeup near one of the positive streamer tips. At this tip the field is locally enhanced to $E/N \geq 1200$ Td, and the plasma irregularity at the tip can be identified. We believe that this irregularity is caused by the low amount of photoionization, in which the incoming avalanches that grow toward the streamer tips lead to a fine-grained local field enhancement.

3.4. Positive streamers with varying photoionization

We now consider the evolution of positive streamers when we vary the amount of photoionization to $\nu_q = 0.1$ and $\nu_q = 0.01$. We first ran simulations with $V = 25$ kV using these parameters, but at this voltage we did not observe propagating streamers. Recalling that the streamer propagation field was 0.8 – 1 kV mm $^{-1}$ with $\nu_q = 1$, we find that the streamer propagation field increases to at least 1 – 1.2 kV mm $^{-1}$ with $\nu_q = 0.1$. This is closer to the experimentally reported propagation field at 1 bar pressure which is 1.2 – 1.3 kV mm $^{-1}$ [7].

Next, computer simulations using a slightly higher applied voltage of $V = 30$ kV showed that propagating streamers did not appear with $\nu_q = 0.01$, but fully developed using $\nu_q = 0.1$. Figure 16 shows the evolution of this discharge, where the baseline simulation ($\nu_q = 1$) is included for the sake of comparison. For the simulation with $\nu_q = 0.1$ the positive streamer propagates at about half the velocity of the baseline simulation, corresponding to a velocity of approximately 0.1 – 0.2 mm ns $^{-1}$. Bagheri *et al* [10] recently reported that the dynamics of CO $_2$ streamers are quite insensitive to the amount of photoionization. However, an important distinction in our work is that electrons and photons are treated in full 3D with discrete particles, whereas Bagheri *et al* [10] treat electrons as a fluid and photoionization using a uniform background density. In our case, the discharge is also highly irregular with a higher plasma density in the filaments, which lies in the range $n_e = 10^{21}$ – 10^{22} m $^{-3}$. In the baseline simulation the plasma density in the channels was typically 10^{20} – 10^{21} m $^{-3}$. The corresponding field at the positive streamer tips were also higher, ranging up to 2000 Td for the filaments with the smallest diameters.

Another difference between the streamer evolution with $\nu_q = 0.1$ and $\nu_q = 1$ is that as the amount of photoionization is lowered the streamer grows even more irregularly. A qualitative demonstration of this is given in figure 17 which shows a closeup of the plasma density in the vicinity of the anode. The baseline data ($\nu_q = 1$) in this figure corresponds to the data at $t = 40$ ns in figure 16. Electron density fluctuations can be seen for the simulation with $\nu_q = 1$, which manifests as a fuzziness in the plasma density in the channels. This irregularity is due to individually incoming avalanches, caused by stochastic fluctuations due to photoionization at the front of the discharge. For the simulation with $\nu_q = 0.1$ this feature

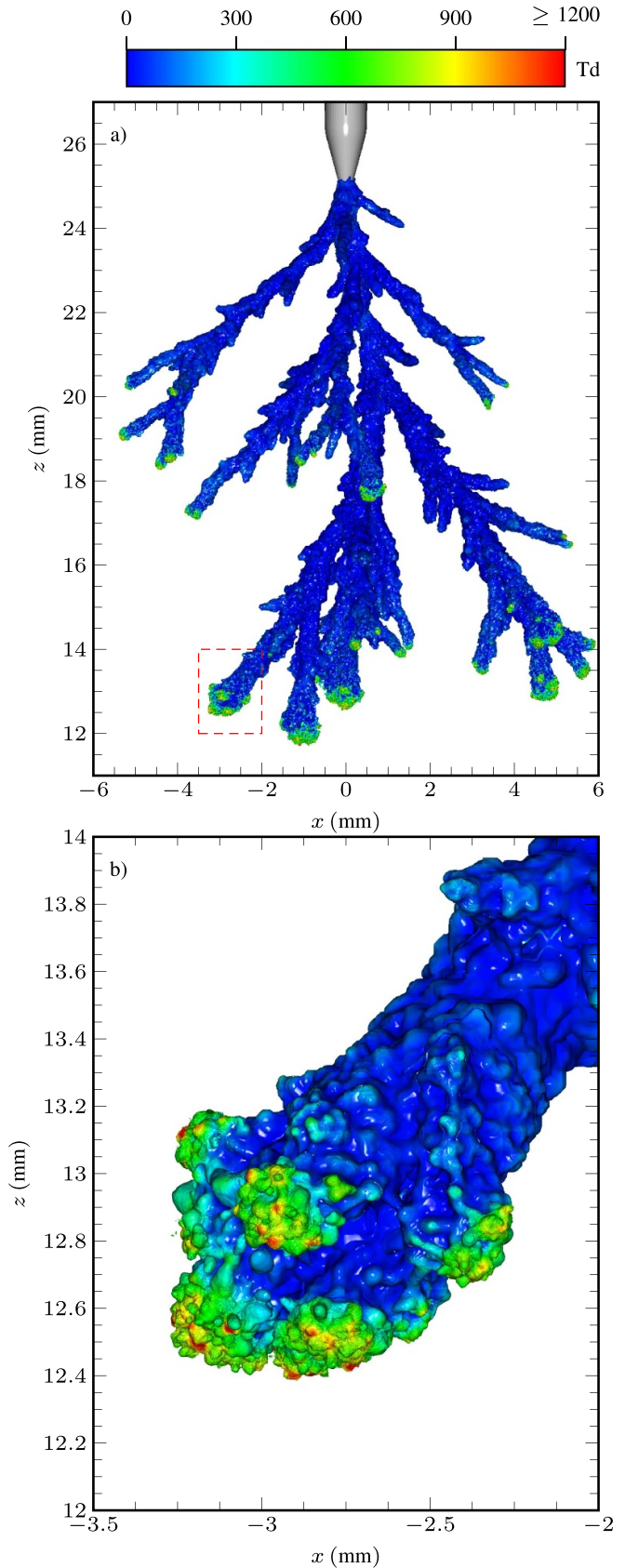


Figure 15. Isosurface $n_e = 10^{18} \text{ m}^{-3}$ for $V = 30$ kV after $t = 56$ ns. The surface is colored by the reduced electric field E/N . (a) Full view. (b) Closeup of the indicated region from (a).

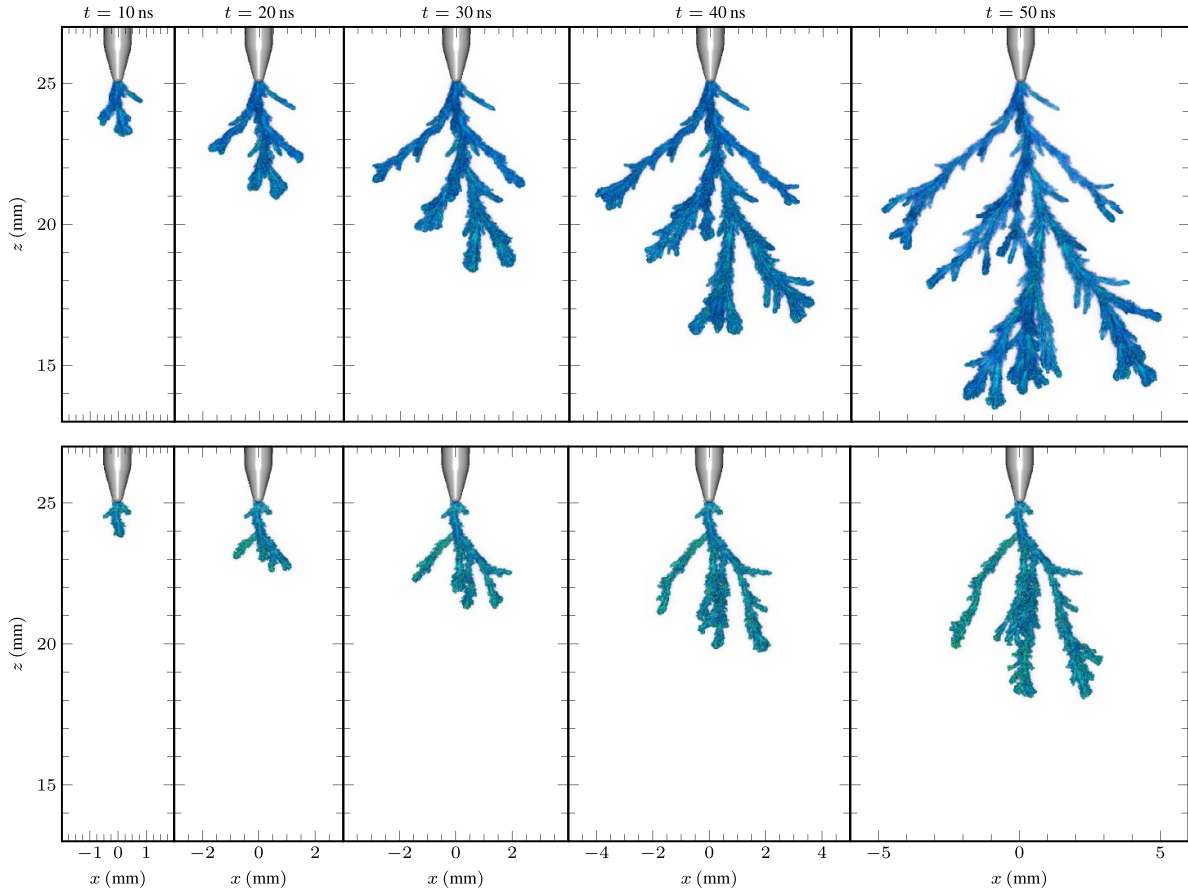


Figure 16. Comparison of positive streamers using an applied voltage $V = 30\text{ kV}$ with $\nu_q = 1$ (top row) and $\nu_q = 0.1$ (bottom row).

is much more pronounced, and individual avalanches can be identified.

3.4.1. The role of photoionization in CO_2 . Despite our initial underestimation of the positive streamer propagation field, we find that positive streamers in CO_2 require substantially higher background fields than positive streamers in air. The breakdown field in CO_2 is around 86 Td while in air the corresponding value is approximately 120 Td , so the breakdown field of CO_2 is only 71% that of air. However, positive streamers in atmospheric air can propagate if the average background field is greater than 0.5 kV mm^{-1} , but positive streamers in CO_2 require background fields greater than 1 kV mm^{-1} . As we showed, the internal field in positive streamer channels is about the same in CO_2 and air, which implies that positive streamers of similar lengths in air and CO_2 carry the same electric potential at their tips. The comparatively large difference in propagation fields in these two gases must therefore be due to conditions at the streamer head rather than conditions inside the streamer channels. Our calculations showed that an increasingly higher voltage is required for propagating positive streamers when the amount of photoionization is lowered, which suggests that the higher propagation field for positive CO_2 streamers could be due to photoionization mechanisms at the streamer tip. Production of ionizing photons in CO_2 is, relatively speaking, lower than

in air. Furthermore, in CO_2 most of the ionizing photons are absorbed very close to the streamer head, with a mean absorption distance on the order of $30\text{ }\mu\text{m}$. Ionizing photons in air propagate longer before they are absorbed, up to 2 mm . This difference in absorption length implies that free electrons that appear due to ionizing radiation in air multiply exponentially over a longer distance than corresponding free electrons in CO_2 . Since positive streamers grow due to incoming electron avalanches, and the size of these avalanches depend on where the free electrons initially appeared, a shorter absorption length effectively leads to a weaker photoionization coupling.

Experimentally, Seeger *et al* [7] found that the pressure-reduced streamer propagation field for negative CO_2 streamers is constant. In other words, if the pressure is doubled then the minimum applied voltage that is necessary in order to initiate and propagate negative streamers is also doubled. For positive streamers, however, the authors observed the same behavior that is commonly observed in air: the pressure-reduced streamer propagation field grows with pressure. This implies that if the pressure is doubled, the applied voltage must be more than doubled in order to initiate and propagate a positive streamer discharge. Based on the observations made above, we conjecture that this is caused by a reduction in the photoionization level at higher pressures, potentially due to collisional quenching of the EUV-emitting fragments involved in the photoionization process.

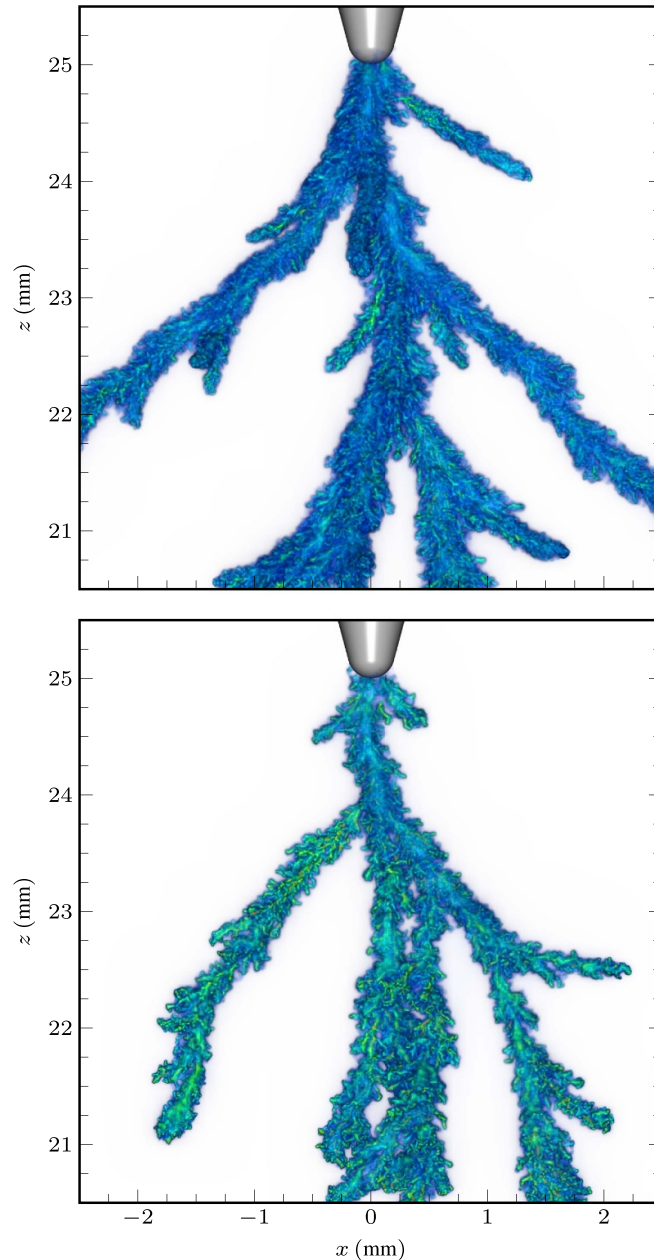


Figure 17. Closeup of the irregularity of positive streamers using an applied voltage $V = 30\text{ kV}$ after $t = 40\text{ ns}$, using $\nu_q = 1$ (top) and $\nu_q = 0.1$ (bottom).

4. Conclusion

4.1. Summary

We have presented a 3D computational study of positive and negative streamer discharges in pure CO_2 , using a microscopic drift-diffusion particle model based on KMC. From the transport data we showed that the existence of a local maximum in the effective attachment rate affects the conductivity, and thus electric field, in the streamer channels. The reduction in the conductivity leads to a corresponding increase in the electric field. This occurs on the timescale of 20 ns for $E/N \approx 70\text{ Td}$ at atmospheric pressure, and thus took place on the time scale

of our computer simulations. We suggest that this mechanism is analogous to the attachment instability in air [16], and that it may play an important role in the further evolution of the discharge. In air, the attachment instability is associated with increased optical emission and presumably also increased localized heating in the channel, which to a coarse approximation is given by $\mathbf{E} \cdot \mathbf{J}$ where only \mathbf{J} is constant through a channel. While we have not modeled optical emission nor heating, it is known that the attachment instability is responsible for the long-term optical emission of sprite discharges in the Earth atmosphere (e.g. column glows and beads) [17, 18]. Analogous emissions may thus exist for sprites in atmospheres mainly composed of CO_2 , such as the Venesian atmosphere.

In the computer simulations we observed very high electric fields $E/N \sim 2000$ Td in the cathode sheath and on some positive streamer tips (in particular for lower photoionization levels). We also used a very fine spatial resolution $\Delta x \lesssim 1 \mu\text{m}$. At these conditions, a standard Courant condition for the maximum permissible time step in fluid-based methods is $\Delta t \leq \Delta x / (|v_x| + |v_y| + |v_z|)$, which would imply using time steps below 0.5 ps. This is 20 times shorter than the actual time step we used in our calculations, and would imply taking over 100 000 time steps in our calculations, which would lead to prohibitively expensive calculations. However, the particle-based LFA model does not have a Courant condition, and alleviated the need for such a small time step. A partial reason for the success of this study was due to this feature, as it allowed us to obtain self-consistent solutions for comparatively large 3D streamer discharges without incurring unacceptable computational costs.

4.2. Negative streamers

For negative streamers we obtain a satisfactory agreement with the experiments by Seeger *et al* [7]. Our calculations indicate that the negative streamer propagation field at 1 bar pressure is 1.1–1.2 kV mm⁻¹. The streamer velocity is voltage dependent and ranges between 0.3–0.6 mm ns⁻¹ in our simulations. The minimum streamer diameter was at least 420 μm . Velocities, propagation fields, and radii were in good agreement with experiments. The channel field in negative CO₂ streamer could become quite high, exceeding 70 Td in the channel, which we suggested was due to the attachment instability. Photoionization was shown to be negligible at the negative streamer head, but nonetheless had a major impact on the streamer evolution since it affects the connection of the negative streamer to the cathode.

4.3. Positive streamers

For positive streamers we obtained partial agreement with experiments [7]. The reported streamer propagation field for positive streamers at 1 bar pressure is approximately 1.2–1.3 kV mm⁻¹, whereas our baseline calculations gave a propagation field of 0.8–1 kV mm⁻¹. This discrepancy indicates that we probably overestimated the amount of photoionization in our calculations, which could either be due to disregard of collisional quenching, lack of reliable photoionization data, or extrapolation of the available photoionization data outside of the experimentally obtained range. Although we were unable to answer which of these factors were incorrect, we found that higher voltages were required in order to sustain positive streamer propagation as we reduced the amount of photoionization. The reported photoionization values by Przybylski [24] are sufficient for sustaining positive discharges in CO₂ at 1 bar, despite the fact that photoionization is weaker than in air and that the photons are absorbed very close to the streamer head. The smallest observed positive streamer radius in the computer simulations was approximately 140 μm , and streamers with this radius did not branch,

so they might correspond to the minimal-diameter streamers observed by Seeger *et al* [7].

The positive streamers were slower than the negative streamers, with typical velocities in the range 0.2–0.4 mm ns⁻¹. This is contrary to behavior in air where positive streamers propagate faster than negative streamers [36]. In CO₂, simulations and experiments [7] both show that negative streamers are faster than positive streamers.

4.4. Outlook

We discussed the lack of reliable photoionization data for CO₂, which is in contrast to air where the photoionization process is well identified, and even simplified models provide sufficient accuracy [5]. Part of the reason for this situation is the lack of energy-resolved emission cross sections for the fragmented products that appear when CO₂ molecules are dissociated through electron impact. Experimentally, data is only available at low pressures and it is not known if the reported data by [24] represents total photoionization, or photoionization per steradian Przybylski [2]. In the latter case, the photoionization efficiency $\xi(E/N)$ that we used in this paper needs to be multiplied by a factor of 4π . The usage of our parameter ν_q is then reinterpreted to include the factor of 4π and the role of quenching. Lack of data on the role of collisional quenching of the EUV-emitting fragments was artificially compensated for by reducing photoionization levels by a factor of 10 and 100, respectively. We observed that positive streamers could develop even at such low levels of photoionization, but that their initiation required a higher applied voltage. We speculate that this is at least partially the reason why experiments show that positive polarity is the dominant breakdown mechanism in CO₂ below atmospheric pressure, while negative polarity dominates at higher pressure [7].

Data availability statement

The calculations presented in this paper were performed using the chombo-discharge computer code [12] (git hash 540f105). Although the results included in this paper are stochastic, the input scripts containing simulation parameters and chemistry specifications that were used in this paper are available in both the chombo-discharge results repository at <https://github.com/chombo-discharge/discharge-papers/tree/main/ItoKMC-CO2>, and at the following URL/DOI: <https://doi.org/10.5281/zenodo.10219863>.

Acknowledgment

This study was partially supported by funding from the Research Council of Norway through Grant 319930. The computations were performed on resources provided by UNINETT Sigma2 - the National Infrastructure for High Performance Computing and Data Storage in Norway.

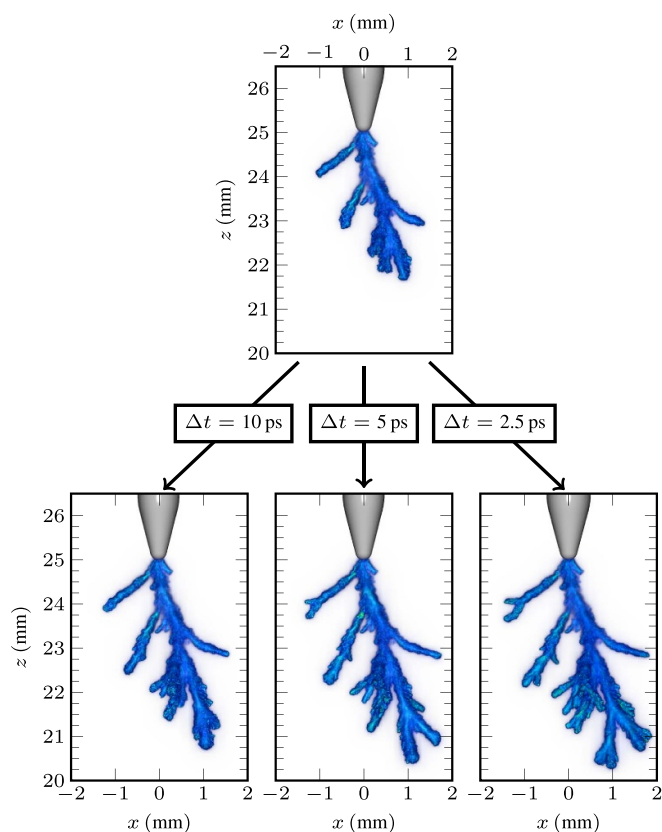


Figure A1. Evolution of the streamers when using different time steps in the computer model. The top figure indicates the starting state of the simulation after $t = 25$ ns, and the bottom row shows the final state after $t = 30$ ns when using various time steps.

Appendix. Grid sensitivity study

In this section we present a sensitivity study of the discharge evolution when using smaller time steps. Our test case considers positive streamers at $V = 25$ kV, corresponding to the top row in figure 12. We first advance the simulation for $t = 25$ ns using our standard time step ($\Delta t = 10$ ps). Next, this state is used as an initial condition for three other simulations that further advanced the simulation to $t = 30$ ns using time steps of $\Delta t = 10$ ps, 5 ps, and 2.5 ps.

The results of the grid sensitivity study are shown in figure A1. A close investigation shows no apparent change in streamer radii, electron densities, and peak fields for these simulations. On the other hand, streamer velocities increase from about 0.2 mm ns^{-1} for $\Delta t = 10$ ps to about 0.27 mm ns^{-1} for $\Delta t = 2.5$ ps. The positive streamer velocities are therefore underestimated by about 25%–30% in our computer simulations.

ORCID iD

R Marskar  <https://orcid.org/0000-0003-1706-9736>

References

- [1] Nijdam S, Teunissen J and Ebert U 2020 The physics of streamer discharge phenomena *Plasma Sources Sci. Technol.* **29** 103001
- [2] Pancheshnyi S 2015 Photoionization produced by low-current discharges in O_2 , air, N_2 and CO_2 *Plasma Sources Sci. Technol.* **24** 015029
- [3] Bagheri B and Teunissen J 2019 The effect of the stochasticity of photoionization on 3D streamer simulations *Plasma Sources Sci. Technol.* **28** 45013
- [4] Marskar R 2020 3D fluid modeling of positive streamer discharges in air with stochastic photoionization *Plasma Sources Sci. Technol.* **29** 055007
- [5] Wang Z, Dijcks S, Guo Y, van der Leege M, Sun A, Ebert U, Nijdam S and Teunissen J 2023 Quantitative modeling of streamer discharge branching in air *Plasma Sources Sci. Technol.* **32** 085007
- [6] Briels T M, Kos J, Winands G J, Veldhuizen E M V and Ebert U 2008 Positive and negative streamers in ambient air: measuring diameter, velocity and dissipated energy *J. Phys. D: Appl. Phys.* **41** 234004
- [7] Seeger M, Avaheden J, Pancheshnyi S and Votteler T 2017 Streamer parameters and breakdown in CO_2 *J. Phys. D: Appl. Phys.* **50** 015207
- [8] Mirpour S and Nijdam S 2022 Investigating CO_2 streamer inception in repetitive pulsed discharges *Plasma Sources Sci. Technol.* **31** 055007
- [9] Levko D, Pachuilo M and Raja L L 2017 Particle-in-cell modeling of streamer branching in CO_2 gas *J. Phys. D: Appl. Phys.* **50** 354004
- [10] Bagheri B, Teunissen J and Ebert U 2020 Simulation of positive streamers in CO_2 and in air: the role of photoionization or other electron sources *Plasma Sources Sci. Technol.* **29** 125021
- [11] Marskar R 2023 Stochastic and self-consistent 3D modeling of streamer discharge trees with kinetic Monte Carlo (arXiv:2307.01797)
- [12] Marskar R 2023 Chombo-discharge: an amr code for gas discharge simulations in complex geometries *J. Open Source Softw.* **8** 5335
- [13] Gillespie D T 2007 Stochastic simulation of chemical kinetics *Annu. Rev. Phys. Chem.* **58** 35–55
- [14] Hagelaar G J and Pitchford L C 2005 Solving the Boltzmann equation to obtain electron transport coefficients and rate coefficients for fluid models *Plasma Sources Sci. Technol.* **14** 722–33
- [15] 2023 Phelps database (available at: www.lxcat.net/Phelps)
- [16] Douglas-Hamilton D H and Mani S A 1973 An electron attachment plasma instability *Appl. Phys. Lett.* **23** 508–10
- [17] Luque A, Stenbaek-Nielsen H C, McHarg M G and Haaland R K 2016 Sprite beads and glows arising from the attachment instability in streamer channels *J. Geophys. Res.: Space Phys.* **121** 2431–49
- [18] Marskar R 2023 Genesis of column sprites: formation mechanisms and optical structures (arXiv:2310.08254)
- [19] Malagón-Romero A and Luque A 2019 Spontaneous emergence of space stems ahead of negative leaders in lightning and long sparks *Geophys. Res. Lett.* **46** 4029–38
- [20] Kochkin P, Lehtinen N, Deursen A P V and Østgaard N 2016 Pilot system development in metre-scale laboratory discharge *J. Phys. D: Appl. Phys.* **49** 425203
- [21] Kochkin P O, Deursen A P V and Ebert U 2014 Experimental study of the spatio-temporal development of metre-scale negative discharge in air *J. Phys. D: Appl. Phys.* **47** 145203
- [22] Stephens J, Abide M, Fierro A and Neuber A 2018 Practical considerations for modeling streamer discharges in air

- with radiation transport *Plasma Sources Sci. Technol.* **27** 075007
- [23] Kanik I, Ajello J M and James G K 1993 Extreme ultraviolet emission spectrum of CO₂ induced by electron impact at 200 eV *Chem. Phys. Lett.* **211** 523–8
- [24] Przybylski A 1962 Untersuchung über die gasionisierende strahlung einer entladung II *Z. Phys.* **168** 504–15
- [25] Ventzek P L G, Hoekstra R J and Kushner M 1994 Two-dimensional modeling of high plasma density inductively coupled sources for materials processing *J. Vac. Sci. Technol. B* **12** 461
- [26] Marskar R 2019 An adaptive Cartesian embedded boundary approach for fluid simulations of two- and three-dimensional low temperature plasma filaments in complex geometries *J. Comput. Phys.* **388** 624–54
- [27] Marskar R 2019 Adaptive multiscale methods for 3D streamer discharges in air *Plasma Res. Express* **1** 015011
- [28] Pancheshnyi S, Nudnova M and Starikovskii A 2005 Development of a cathode-directed streamer discharge in air at different pressures: experiment and comparison with direct numerical simulation *Phys. Rev. E* **71** 016407
- [29] Luque A, Ratushnaya V and Ebert U 2008 Positive and negative streamers in ambient air: modelling evolution and velocities *J. Phys. D: Appl. Phys.* **41** 234005
- [30] Meyer H K, Marskar R, Gjerdal H and Mauseth F 2020 Streamer propagation along a profiled dielectric surface *Plasma Sources Sci. Technol.* **29** 115015
- [31] Meyer H K H, Marskar R and Mauseth F 2022 Evolution of positive streamers in air over non-planar dielectrics: experiments and simulations *Plasma Sources Sci. Technol.* **31** 114006
- [32] Meyer H K, Mauseth F, Marskar R, Pedersen A and Blaszczyk A 2019 Streamer and surface charge dynamics in non-uniform air gaps with a dielectric barrier *IEEE Trans. Dielectr. Electr. Insul.* **26** 1163–71
- [33] Luque A, Ebert U, Montijn C and Hundsdoerfer W 2007 Photoionization in negative streamers: fast computations and two propagation modes *Appl. Phys. Lett.* **90** 081501
- [34] Starikovskiy A Y and Aleksandrov N L 2020 How pulse polarity and photoionization control streamer discharge development in long air gaps *Plasma Sources Sci. Technol.* **29** 075004
- [35] Naidis G V 2009 Positive and negative streamers in air: velocity-diameter relation *Phys. Rev. E* **79** 057401
- [36] Briels T M, Veldhuizen E M V and Ebert U 2008 Positive streamers in air and nitrogen of varying density: experiments on similarity laws *J. Phys. D: Appl. Phys.* **41** 234008